Title

How Bulk Sensitive is Hard X-ray Photoelectron Spectroscopy: Accounting for the Cathode-Electrolyte Interface when Addressing Oxygen Redox.

Journal

The journal of physical chemistry letters, 11(6)

ISSN

1948-7185

Authors

Lebens-Higgins, Zachary W
Chung, Hyeseung
Zuba, Mateusz J
et al.

Publication Date

2020-03-01

DOI

10.1021/acs.jpclett.0c00229

Peer reviewed

How Bulk Sensitive is Hard X-ray Photoelectron Spectroscopy: Accounting for the Cathode−Electrolyte Interface when Addressing Oxygen Redox

Zachary W. Lebens-Higgins, Hyeseung Chung, Mateusz J. Zuba, Jatinkumar Rana, Yixuan Li, Nicholas V. Faenza, Nathalie Pereira, Bryan D. McCloskey, Fanny Rodolakis, Wanli Yang, M. Stanley Whittingham, Glenn G. Amatucci, Ying Shirley Meng, Tien-Lin Lee, and Louis F. J. Piper*

ABSTRACT: Sensitivity to the "bulk" oxygen core orbital makes hard X-ray photoelectron spectroscopy (HAXPES) an appealing technique for studying oxygen redox candidates. Various studies have reported an additional O 1s peak (530−531 eV) at high voltages, which has been considered a direct signature of the bulk oxygen redox process. Here, we find the emergence of a 530.4 eV O 1s HAXPES peak for three model cathodes—Li_2MnO_3, Li-rich NMC, and NMC 442—that shows no clear link to oxygen redox. Instead, the 530.4 eV peak for these three systems is attributed to transition metal reduction and electrolyte decomposition in the near-surface region. Claims of oxygen redox relying on photoelectron spectroscopy must explicitly account for the surface sensitivity of this technique and the extent of the cathode degradation layer.

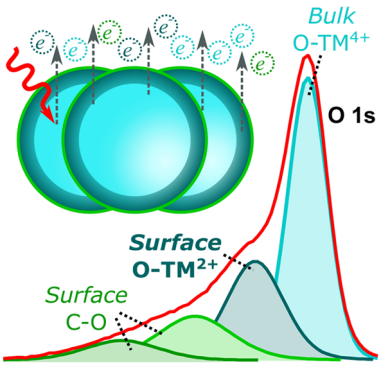

Alkali-rich oxides have gained significant attention as next-generation battery cathodes in recent years, achieving reversible capacities beyond 270 mAh/g.[1−3] In comparison to conventional layered oxides ($LiMO_2$), alkali-rich cathodes deliver excess capacity beyond what is expected from traditional transition metal (TM) redox couples that is widely attributed to oxygen redox.[3,4] Interest in utilizing oxygen redox capacity has generated research into a variety of novel 3d, 4d, and 5d compounds[3,5−7] and intercalation structures.[7,8] Li- and Mn-rich Ni/Co/Mn layered oxides (LR-NMC) remain at the forefront of this field for achieving high performance[9,10] and for investigating the fundamental electrochemistry of alkali-rich oxides.[11−13] Indeed, recent studies focusing on LR-NMC cathodes have revealed mechanisms that contribute to the large hysteresis[11,13] and voltage decay[12] found across anionic redox compounds.[3,6] Direct insight into oxidized oxygen has primarily relied on two techniques: X-ray photoelectron spectroscopy (XPS) at the O 1s region[14−16] and resonant inelastic X-ray scattering (RIXS) at the O K-edge.[11,17,18] Unlike RIXS which requires a bright variable energy X-ray synchrotron source, XPS is a common lab-based technique resulting in its extensive use for studying oxygen redox candidates.[5,15,19−25]

Lab-based XPS is inherently surface-sensitive (probing depth <5 nm) with a large portion of the signal coming from electrolyte decomposition species at the cathode surface. Hard X-ray photoelectron spectroscopy (HAXPES) has been used to overcome this limitation with probing depths >20 nm that allow for increased sensitivity to the "bulk" oxygen core orbitals.[16,26,27] In these measurements, the emergence of an O 1s peak in the same binding energy window (530−531 eV) as common peroxides, e.g., Na_2O_2[28] and Li_2O_2,[29] has been considered a signature of oxygen redox. This method has to this point been seen as a quantitative probe of bulk oxidized oxygen states for identifying the onset and reversibility of oxygen redox.

In this study, we focus on HAXPES O 1s measurements to address this interpretation for three layered oxide cathodes: Li_2MnO_3,[30] $Li[Li_{0.144}Ni_{0.136}Mn_{0.544}Co_{0.136}]O_2$ (LR-NMC),[31] and $LiNi_{0.4}Mn_{0.4}Co_{0.2}O_2$ (NMC 442).[32] All three systems (Li-rich and conventional) show the emergence of an additional HAXPES O 1s peak (530.4 eV peak) that is found to be inconsistent with the expected oxygen redox contribution. Indeed, a stronger 530.4 eV O 1s peak is observed for a conventional layered oxide cathode (NMC 442) than for LR-NMC at high states of charge. When accounting for the surface sensitivity of HAXPES, our results reveal how a

combination of electrolyte decomposition species and near-surface TM-reduction contribute to the evolution of a 530.4 eV peak for oxide cathodes.

For our focus on the O 1s core region, we utilized photon-dependent XPS at 0.8, 1.5, and 6 keV with electron inelastic mean free paths (IMFPs) of 0.8, 1.6, and 7.8 nm, respectively, calculated using the TPP-2 M method[33] from the NIST electron IMFP database.[34] The corresponding attenuation profiles[35] (photoelectron signal versus depth) for these three photon energies are given in Figure 1a. The 0.8 and 1.5 keV

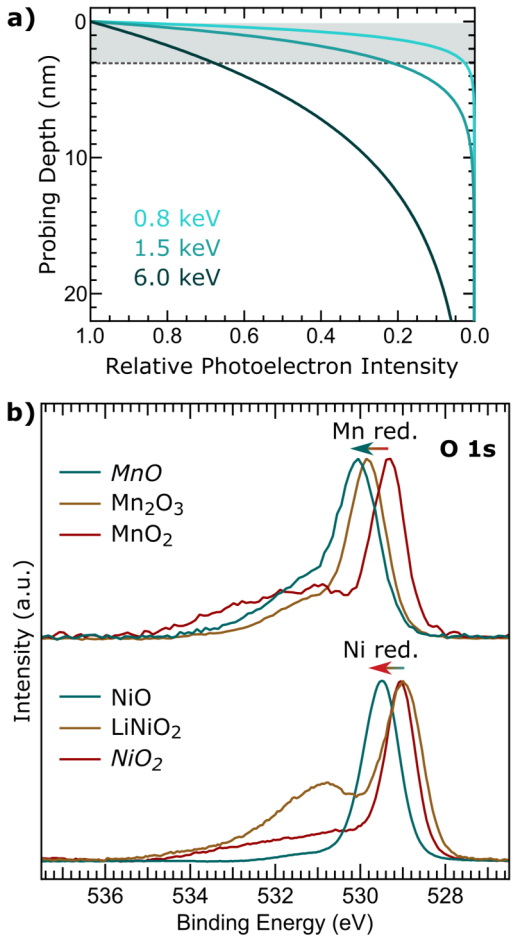

Figure 1. (a) Relative photoelectron signal versus depth at 0.8, 1.5, and 6 keV. The gray shaded region highlights the contribution from the top 3 nm. (b) HAXPES O 1s spectra for manganese (MnO, Mn_2O_3, and MnO_2) and nickel (NiO, $LiNiO_2$, and NiO_2) oxide references. Manganese and nickel oxides were measured at 1.5 and 6 keV, respectively.

measurements are highly surface-sensitive as over 85% of the signal originates from the top 3 nm. For 6 keV HAXPES, the contribution from the top 3 nm is reduced to 30% and the overall probing depth is ~23 nm (3× the IMFP), the region in which 95% of the signal originates from. Yet, these HAXPES measurements still have a significant contribution from the cathode−electrolyte interface given that electrolyte decomposition and TM-reduction/densification is often on the order of a few nanometers for oxide cathodes.[36−40]

Beyond considering the attenuation profile, we explicitly examined the O 1s spectra for manganese and nickel oxide references (Figure 1b). The lattice oxygen peaks for commercial MnO (Mn^{2+}), Mn_2O_3 (Mn^{3+}), and MnO_2 (Mn^{4+}) are found at 530.05, 529.8, and 529.35 eV, respectively, matching with previously reported values.[41,42] The MnO reference may be partially oxidized (Figure S1) resulting in only a small shift of the O 1s peak beyond Mn_2O_3.[43] Nickel references consisted of a NiO (Ni^{2+}) epitaxial film and $LiNiO_2$ electrodes charged to 3.6 V ($LiNiO_2$) and 4.75 V (NiO_2). The first charge of $LiNiO_2$ resulted in a charge capacity of 286 mAh/g, suggesting the material is near full delithiation (Figure S2). The nickel references were measured with HAXPES to minimize the contribution of carbonates that tend to form on lithiated nickel-rich oxides.[44,45] The Ni−O peaks for NiO, $LiNiO_2$, and NiO_2 are found at 529.5, 529.0, and 529.05 eV, respectively. From these reference measurements, we find the lattice O 1s peak shifts to higher binding energies as a direct result of the reduction of surrounding TMs. Additional discussion of the fundamental contributions to the core oribital peak position[46,47] is given in supplementary note 1.

Following these insights, we turn to HAXPES characterization of Li-rich and conventional layered oxide cathodes. Electrode preparation and cell testing details are given in the Supporting Information along with scanning electron microscopy images of pristine materials (Figure S3). First, we focus on Li_2MnO_3 that displays first charge and discharge capacities of 336 and 168 mAh/g, respectively (Figure 2a). In our recent study, this high charge capacity was found to primarily originate from oxygen loss and side reactions with limited contribution from reversible oxygen redox.[30] Indeed, highly charged Li_2MnO_3 displays no RIXS features associated with the formation of stabilized oxidized oxygen states.[30,48] HAXPES measurements were conducted on pristine Li_2MnO_3 and three electrodes, beginning of charge (4.55 V), end of charge (5.00 V), and end of discharge (2.00 V), prepared with 75% active material, 15% carbon black (CB), and 10% PVdF binder. The Li 1s and Mn 3p regions for these samples are given in Figure 2b. The Li 1s peak at 54.3 eV is associated with lithium in the lattice and increases (decreases) during charge (discharge). This peak is detectable at 5.00 V, indicating some lithium remains in the lattice at the end of charge. In the Mn 3p, there is an increase in the lower binding energy shoulder at 48 eV between the pristine material and 4.55 V electrode. Ilton et al.[43] identified the main Mn 3p peak for Mn^{4+}, Mn^{3+}, and Mn^{2+} references at 49.94, 48.79, 47.46 eV, respectively. Comparison of these values to the Li_2MnO_3 electrodes indicates that the lower binding energy shoulder is consistent with the formation of a Mn-reduced surface layer. During the first cycle, the Mn 3p line shape never fully returns to the pristine material, indicating a partially reduced Mn surface region remains throughout the throughout the first cycle. This conclusion is supported by complementary HAXPES of the Mn 2p core region (Figure S1). These results are consistent with previous observations of extensive oxygen loss[30,49] and surface reduction[30,39] for Li_2MnO_3.

Focusing on the O 1s core region, we conducted peak fits for each of the Li_2MnO_3 samples (Figure 2c). For pristine Li_2MnO_3, the main lattice peak is at 529.35 and there is a minor peak at ~530.4 eV. During the first cycle, higher binding energy features (>531 eV) are found to emerge that are associated with electrolyte decomposition species including C=O (531.7 eV) and C−O (533.25 eV) environments from solvent decomposition.[50,51] These species are particularly prevalent in 1.5 keV measurements (Figure S4).

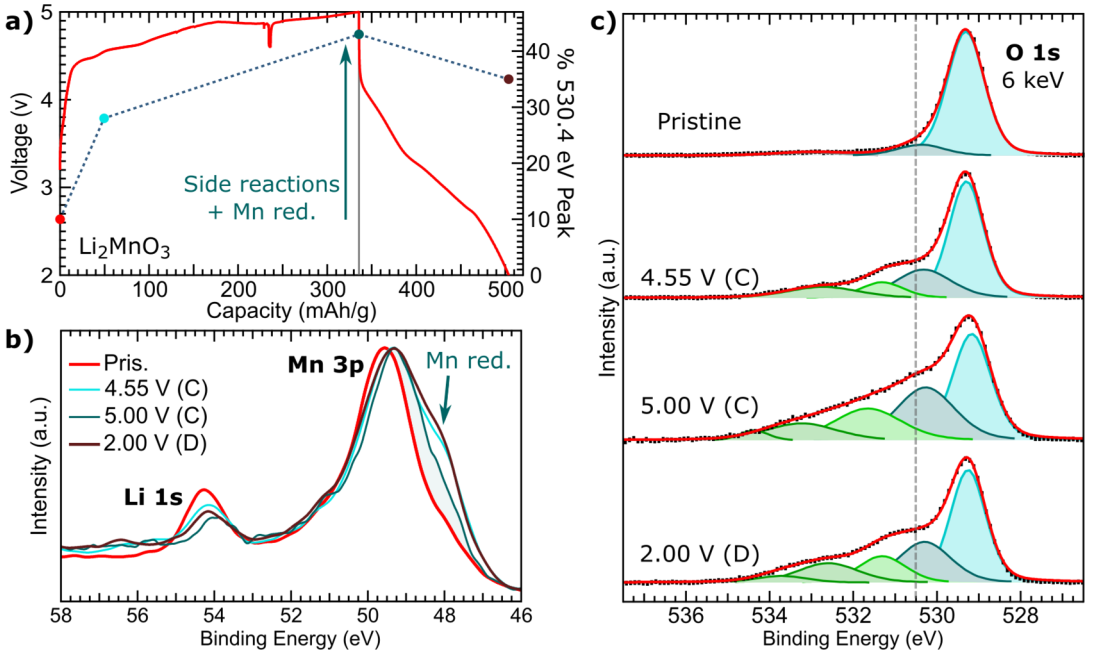

Figure 2. (a) First cycle electrochemistry for Li_2MnO_3 charged (C) to 5.00 V and then discharged (D) to 2.00 V. (b) Li 1s and Mn 3p core regions and (c) O 1s peak fits at 6 keV of pristine Li_2MnO_3 and electrodes charged to 4.55 and 5.00 V and discharged to 2.00 V. The gray line in panel c highlights the 530.4 eV peak. The variation in this peak is compared to the electrochemistry in panel a.

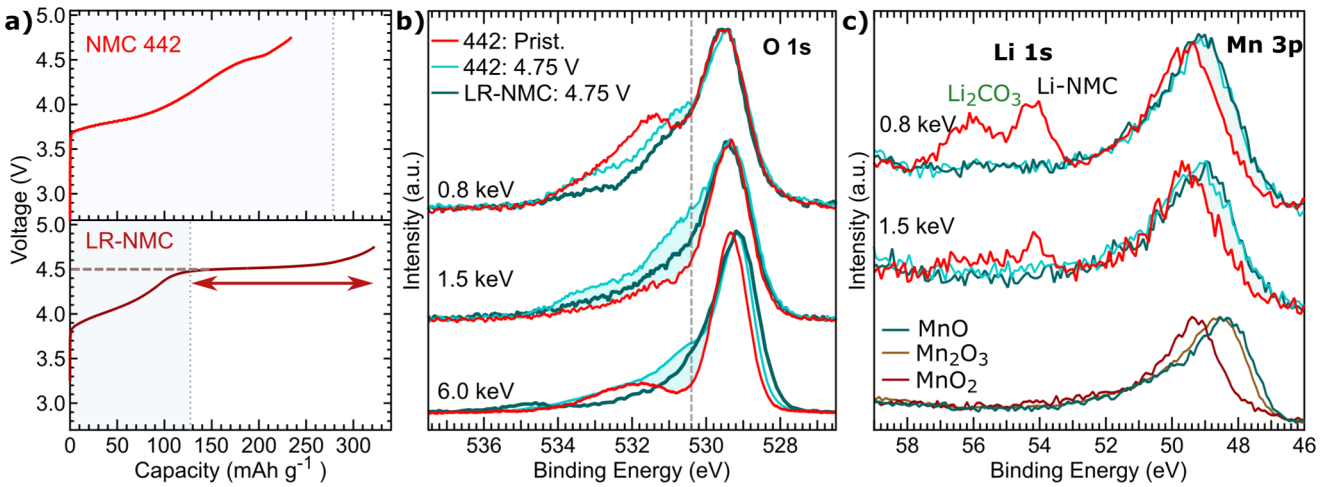

Figure 3. (a) First charge of NMC 442 and LR-NMC to 4.75 V. (b) O 1s measured at 0.8, 1.5, and 6 keV and (c) Li 1s and Mn 3p core regions at 0.8 and 1.5 keV for NMC 442 and LR-NMC 4.75 V electrodes compared to a pristine NMC 442 electrode. For the O 1s, the shading indicates the additional 530.4 eV peak that is present at high voltages for the LR-NMC and NMC 442. For the Mn 3p, reference Mn−O (Mn^{2+}), Mn_2O_3 (Mn^{3+}), and MnO_2 (Mn^{4+}) spectra relate the Mn-valence to the Mn 3p peak position.

Of particular interest is the evolution of the 530.4 eV peak at the same binding energy as assigned to "peroxo-like" oxygen redox features in other systems.[15,16,26] The percentage of this peak versus the main lattice oxygen peak [$O_{530.4}$/($O_{530.4}$+$O_{529.35}$)] is plotted alongside the electrochemistry in Figure 2a. This peak increases at the start of charge (4.55 V) and after charging to 5.00 V but shows only a small decrease after discharge. The limited reversibility, combined with the extensive near-surface Mn-reduction (Figure 2b) and absence of oxidized oxygen RIXS features,[30,48] suggest the 530.4 eV peak is not associated with lattice oxygen redox for Li_2MnO_3. One possible assignment for this peak is surface Mn-reduction given its similar binding energy to lattice Mn^{3+}/Mn^{2+} O 1s peaks (Figure 1b), concurrent increase with Mn-reduction at 4.55 V, and limited reversibility. There is a continued increase of the 530.4 eV peak above 4.55 V with no concurrent increase in Mn-reduction, suggesting that electrolyte decomposition species may also contribute. This could include O−H groups[28,41] that have been assigned around this binding energy for other battery materials.[52] The formation of hydroxide species would not be unexpected for Li_2MnO_3.[53] These results indicate that a combination of electrolyte decomposition and TM-reduction account for the evolution of the 530.4 eV peak for Li_2MnO_3.

While Li_2MnO_3 is a clear example of a 530−531 eV peak that cannot be attributed to oxidized oxygen, Li_2MnO_3 was tested with a high cutoff voltage (5.00 V) and undergoes more extensive oxygen loss/TM-reduction than Li-rich and conven-

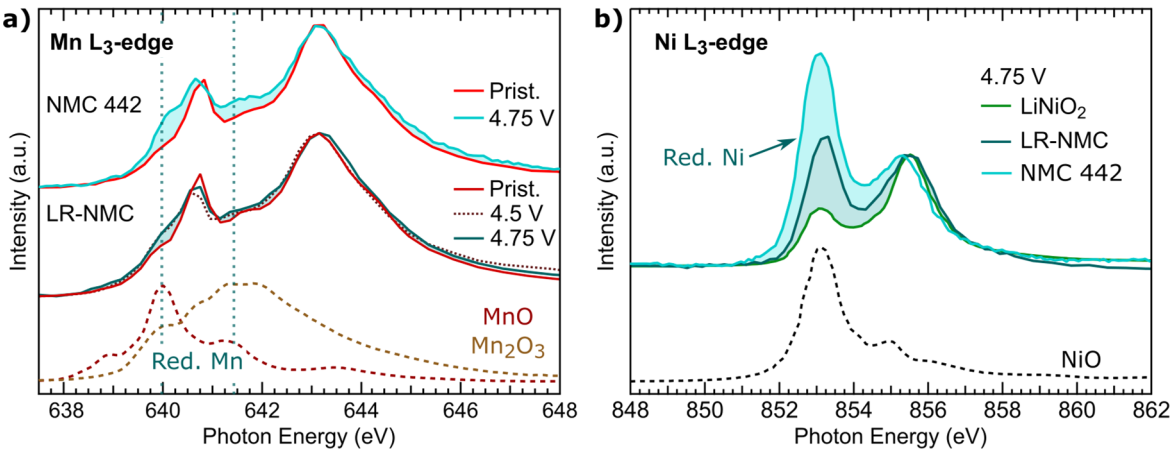

Figure 4. (a) Mn L-edge and (b) Ni L_3-edge in total electron yield (TEY) mode for NMC 442 pristine and 4.75 V, and LR-NMC pristine, 4.5 V, and 4.75 V electrodes. Mn L_3-edge spectra for MnO and Mn_2O_3 and Ni L_3-edge spectra for a NiO epitaxial thin film and $LiNiO_2$ 4.75 V electrode (Ni^{4+}) are included for reference. Shadings in panels a and b highlight changes that result from TM-reduction.

tional NMC layered oxides.[30,49,54] As such, we conducted additional HAXPES measurements on Li-rich NMC and NMC 442 cathodes. For these systems, minimal additives (CB/PVdF) were used compared to Li_2MnO_3 (see the Supporting Information) that did not compromise the electrochemistry. This will improve the direct sensitivity of the measurements to the active material. The electrochemical curves of the first charge of NMC 442 and LR-NMC to 4.75 V (vs Li-metal) at 10 mA/g and at room temperature (RT) are given in Figure 3a. NMC 442 exhibits a charge capacity of 234 mAh/g that is attributed to traditional Ni/Co redox couples (gray shading). The LR-NMC exhibits the typical first charge activation plateau of oxygen redox cathodes and a higher capacity of 322 mAh/g. Although O K-edge RIXS studies have demonstrated the emergence of oxidized oxygen states in $LiMO_2$ cathodes at high degrees of delithiation,[55] more prominent RIXS features are observed for LR-NMC where the capacity is twice what is expected from traditional TM redox couples alone. Our previous study conducted on this LR-NMC system displayed clear O K-edge RIXS features at 4.75 V associated with oxidized oxygen states.[31]

Photon-dependent XPS measurements of the O 1s, Li 1s, and Mn 3p core regions at 0.8, 1.5, and 6 keV of these two systems are shown in Figure 3b,c. The O 1s region is normalized to the main O-NMC lattice peak (529.0 to 530 eV). For the pristine electrode, initial O and Li 1s peaks at 531.4 and 56 eV, respectively, in the 0.8 keV measurements are associated with a thin Li_2CO_3 layer, a typical contaminant on oxide cathodes that breaks down during electrochemical testing.[44,45,54] This accounts for the loss of these O 1s/Li 1s peaks after charging to 4.75 V. The lower-energy Li 1s peak in the pristine material at 54.2 eV is associated with lattice lithium.[51] This peak is below our detection limit after charge directly reflecting delithiation of the NMC electrodes. Compared with Li_2MnO_3 (Figure S4), the LR-NMC and NMC 442 electrodes display minimal higher binding energy C−O/C=O (>531.5 eV) O 1s peaks.[50,51] Instead, the main difference for the electrodes charged to 4.75 V is the formation of a new peak at 530.4 eV. The NMC 442 4.75 V electrode has a stronger 530.4 eV peak than the LR-NMC 4.75 V electrode at all photon energies, including the more bulk-sensitive HAXPES measurements.

Corresponding O 1s peak fits for the NMC electrodes are given in Figure S5 and Table S1. For the 6 keV measurements, the percentage of the 530.4 eV peak relative to the main lattice oxygen peak is 35% and 17% for the NMC 442 and LR-NMC 4.75 V electrodes, respectively. This is opposite what would be expected if this new O 1s peak was solely attributed to oxygen redox. In addition, this peak is partially formed by 4.0 V for NMC 442 (Figure S5), indicating it is not just a high-voltage phenomena. Turning to the manganese environment, we find the Mn 3p shifts to a lower binding energy for the high state of charge (SOC) NMC electrodes compared to the pristine electrode. From comparison with the manganese oxide references, we find that this shift to lower binding energy is consistent with Mn-reduction at the cathode surface. HAXPES measurements of the Ni and Mn core regions show additional evidence of an extended reduced layer forming after charge (Figure S7)

To further gauge the extent of TM reduction, we conducted complementary soft X-ray absorption spectroscopy (sXAS) measurements of the Mn and Ni L_3-edges in electron mode that are well-known to be highly sensitive to the TM oxidation state in the near-surface region.[56,57] For the Mn L_3-edge (Figure 4a), high SOC NMC electrodes are compared to corresponding pristine powders. The pristine compounds are nominally Mn^{4+} with the shading in Figure 4a indicating the extent of Mn-reduction found at higher SOCs. For the LR-NMC electrodes, the Mn-reduction increases up to 4.5 V (start of the high voltage plateau) and shows limited changes along the plateau. A larger increase in the Mn surface reduction is found for the NMC 442 system for the 4.75 V electrode compared to Li-rich NMC. Corresponding fits of the oxidation state are given in Figure S8. For the Ni L_3-edge (Figure 4b), the NMC electrodes are compared to a NiO (Ni^{2+}) reference and a $LiNiO_2$ electrode charged to 4.75 V that nominally matches the Ni^{4+} line shape.[11] The NMC electrodes show a strong Ni^{2+} surface component based on the increase in the Ni L_3-edge peak at 853.1 eV relative to the peak at 855.5 eV (shading in Figure 4b) with the NMC 442 showing more Ni-reduction than LR-NMC. From these sXAS measurements, we found that NMC 442 displays more surface TM reduction than the LR-NMC. This trend matches with the higher O 1s 530.4 eV peak observed for the NMC 442 than for LR-NMC, further

supporting that this O 1s peak forms as a result of surface TM-reduction during the first charge.

From comparison of three layered oxide cathodes, we identified how electrolyte decomposition and TM-reduction can contribute to the evolution of an O 1s peak between 530 and 531 eV. The presence of this peak at 4.0 V for NMC 442 is consistent with the onset of TM surface reduction around 3.9 V identified indirectly with differential electrochemical mass spectroscopy (DEMS).[58] This onset was found to coincide with the loss of Li_2CO_3 identified from CO_2 gas release and post-titration measurements.[58] These are just two of the changes in the cathode−electrolyte interface composition during the first cycle that have been identified with DEMS and XPS/HAXPES[31,54,58] that need to be accounted for when addressing bulk redox mechanisms with techniques that are inherently surface-sensitive.

Our interpretation of the O 1s spectra may account for previous observations for alkali-rich oxides. For example, Uchimoto et al.[26] reported a strong additional peak in their O 1s HAXPES spectra of LR-NMC before the start of the high-voltage plateau that persisted after discharge, showing no clear correlation to the expected oxygen redox capacity. This HAXPES O 1s evolution is in contrast to bulk-sensitive STXM and RIXS techniques, where assignments of oxidized lattice oxygen do correlate with capacity.[11,18] Our work highlights the importance of linking structural and electronic probes with the electrochemistry in order to establish a technique as a reliable oxygen redox probe.

AUTHOR INFORMATION

Corresponding Author

Louis F. J. Piper − *Department of Physics, Applied Physics and Astronomy and Materials Science & Engineering, Binghamton University, Binghamton, New York 13902, United States;* orcid.org/0000-0002-3421-3210; Email: lpiper@binghamton.edu

Authors

Zachary W. Lebens-Higgins − *Department of Physics, Applied Physics and Astronomy, Binghamton University, Binghamton, New York 13902, United States;* orcid.org/0000-0001-5978-7926

Hyeseung Chung − *Department of NanoEngineering, University of California San Diego, La Jolla, California 92093, United States*

Mateusz J. Zuba − *Materials Science & Engineering, Binghamton University, Binghamton, New York 13902, United States*

Jatinkumar Rana − *Materials Science & Engineering, Binghamton University, Binghamton, New York 13902, United States;* orcid.org/0000-0002-3552-2453

Yixuan Li − *Department of NanoEngineering, University of California San Diego, La Jolla, California 92093, United States*

Nicholas V. Faenza − *Energy Storage Research Group, Department of Materials Science and Engineering, Rutgers University, North Brunswick, New Jersey 08902, United States;* orcid.org/0000-0002-2620-4592

Nathalie Pereira − *Energy Storage Research Group, Department of Materials Science and Engineering, Rutgers University, North Brunswick, New Jersey 08902, United States*

Bryan D. McCloskey − *Energy Storage and Distributed Resources Division, Lawrence Berkeley National Laboratory, Berkeley, California 94720, United States; Department of Chemical and Biomolecular Engineering, University of California Berkeley, Berkeley, California 94720, United States;* orcid.org/0000-0001-6599-2336

Fanny Rodolakis − *Argonne National Laboratory, Argonne, Illinois 60439, United States*

Wanli Yang − *Advanced Light Source, Lawrence Berkeley National Laboratory, Berkeley, California 94720, United States;* orcid.org/0000-0003-0666-8063

M. Stanley Whittingham − *Materials Science & Engineering, Binghamton University, Binghamton, New York 13902, United States;* orcid.org/0000-0002-5039-9334

Glenn G. Amatucci − *Energy Storage Research Group, Department of Materials Science and Engineering, Rutgers University, North Brunswick, New Jersey 08902, United States;* orcid.org/0000-0003-1905-6197

Ying Shirley Meng − *Department of NanoEngineering, University of California San Diego, La Jolla, California 92093, United States;* orcid.org/0000-0001-8936-8845

Tien-Lin Lee − *Diamond Light Source Ltd., Didcot, Oxfordshire OX11 0DE, U.K.*

Complete contact information is available at: https://pubs.acs.org/10.1021/acs.jpclett.0c00229

Notes

The authors declare no competing financial interest.

ACKNOWLEDGMENTS

This work was supported as part of the NorthEast Center for Chemical Energy Storage (NECCES), an Energy Frontier Research Center funded by the U.S. Department of Energy, Office of Science, Office of Basic Energy Sciences under Award No. DE-SC0012583. L.F.J.P and B.D.M. also thank Research Corporation for Science Advancement for funding through the Scialog program. The work at the ALS was supported by the Office of Basic Energy Sciences, of the U.S. Department of Energy under Contract No. DE-AC02-05CH11231. This research used resources of the Advanced Photon Source, a U.S. Department of Energy (DOE) Office of Science User Facility operated for the DOE Office of Science by Argonne National Laboratory under Contract No. DE-AC02-06CH11357; additional support was provided by National Science Foundation under Grant No. DMR-0703406. We acknowledge Diamond Light Source for time on Beamline I09 under Proposals No. SI22250-1 and No. SI22148-1.

REFERENCES

(1) Saubanère, M.; McCalla, E.; Tarascon, J.-M.; Doublet, M.-L. The Intriguing Question of Anionic Redox in High-Energy Density Cathodes for Li-ion Batteries. *Energy Environ. Sci.* **2016**, *9*, 984−991.

(2) Qiu, B.; Zhang, M.; Xia, Y.; Liu, Z.; Meng, Y. S. Understanding and Controlling Anionic Electrochemical Activity in High-Capacity

Oxides for Next Generation Li-Ion Batteries. *Chem. Mater.* **2017**, *29*, 908−915.
(3) Assat, G.; Tarascon, J.-M. Fundamental Understanding and Practical Challenges of Anionic Redox Activity in Li-ion Batteries. *Nat. Energy* **2018**, *3*, 373−386.
(4) Seo, D.-H.; Lee, J.; Urban, A.; Malik, R.; Kang, S.; Ceder, G. The Structural and Chemical Origin of the Oxygen Redox Activity in Layered and Cation-Disordered Li-Excess Cathode aterials. *Nat. Chem.* **2016**, *8*, 692−697.
(5) Sathiya, M.; Ramesha, K.; Rousse, G.; Foix, D.; Gonbeau, D.; Prakash, A. S.; Doublet, M. L.; Hemalatha, K.; Tarascon, J. M. High Performance $Li_2Ru_{1-y}Mn_yO_3$ $(0.2 \leq y \leq 0.8)$ Cathode Materials for Rechargeable Lithium-Ion Batteries: Their Understanding. *Chem. Mater.* **2013**, *25*, 1121−1131.
(6) Sathiya, M.; Abakumov, A. M.; Foix, D.; Rousse, G.; Ramesha, K.; Saubanère, M.; Doublet, M. L.; Vezin, H.; Laisa, C. P.; Prakash, A. S.; Gonbeau, D.; Vantendeloo, G.; Tarascon, J. M. Origin of Voltage Decay in High-Capacity Layered Oxide Electrodes. *Nat. Mater.* **2015**, *14*, 230−238.
(7) Yabuuchi, N.; Nakayama, M.; Takeuchi, M.; Komaba, S.; Hashimoto, Y.; Mukai, T.; Shiiba, H.; Sato, K.; Kobayashi, Y.; Nakao, A.; Yonemura, M.; Yamanaka, K.; Mitsuhara, K.; Ohta, T. Origin of Stabilization and Destabilization in Solid-State Redox Reaction of Oxide Ions for Lithium-Ion Batteries. *Nat. Commun.* **2016**, *7*, 13814.
(8) Yabuuchi, N.; Takeuchi, M.; Nakayama, M.; Shiiba, H.; Ogawa, M.; Nakayama, K.; Ohta, T.; Endo, D.; Ozaki, T.; Inamasu, T.; Sato, K.; Komaba, S. High-Capacity Electrode Materials for Rechargeable Lithium Batteries: Li_3NbO_4-Based System with Cation-Disordered Rocksalt Structure. *Proc. Natl. Acad. Sci. U. S. A.* **2015**, *112*, 7650−7655.
(9) Qiu, B.; Zhang, M.; Wu, L.; Wang, J.; Xia, Y.; Qian, D.; Liu, H.; Hy, S.; Chen, Y.; An, K.; Zhu, Y.; Liu, Z.; Meng, Y. S. Gas-Solid Interfacial Modification of Oxygen Activity in Layered Oxide Cathodes for Lithium-Ion Batteries. *Nat. Commun.* **2016**, *7*, 12108.
(10) Bai, X.; Shen, X.; Zhu, L.; Sun, X.; Liu, Z.; Kong, Q.; Chen, K.; Gao, Y.; Lu, G.; Chen, L.; Wang, Z.; Li, M.; Yu, R.; Banis, M. N.; Liu, S.; Li, W. Surface Doping to Enhance Structural Integrity and Performance of Li-Rich Layered Oxide. *Adv. Energy Mater.* **2018**, *8*, 1802105.
(11) Gent, W. E.; Lim, K.; Liang, Y.; Li, Q.; Barnes, T.; Ahn, S.-J.; Stone, K. H.; Mcintire, M.; Hong, J.; Song, J. H.; Li, Y.; Mehta, A.; Ermon, S.; Tyliszczak, T.; Kilcoyne, D.; Vine, D.; Park, J.-H.; Doo, S.-K.; Toney, M. F.; Yang, W.; Prendergast, D.; Chueh, W. C. Coupling Between Oxygen Redox and Cation Migration Explains Unusual Electrochemistry in lithium-Rich Layered Oxides. *Nat. Commun.* **2017**, *8*, 2091.
(12) Hu, E.; Yu, X.; Lin, R.; Bi, X.; Lu, J.; Bak, S.; Nam, K.-W.; Xin, H. L.; Jaye, C.; Fischer, D. A.; Amine, K.; Yang, X.-Q. Evolution of Redox Couples in Li- and Mn-Rich Cathode Materials and Mitigation of Voltage Fade by Reducing Oxygen Release. *Nat. Energy* **2018**, *3*, 690−698.
(13) Kleiner, K.; Strehle, B.; Baker, A. R.; Day, S. J.; Tang, C. C.; Buchberger, I.; Chesneau, F. F.; Gasteiger, H. A.; Piana, M. Origin of High Capacity and Poor Cycling Stability of Li-Rich Layered Oxides: A Long-Duration in Situ Synchrotron Powder Diffraction Study. *Chem. Mater.* **2018**, *30*, 3656−3667.
(14) Sathiya, M.; Rousse, G.; Ramesha, K.; Laisa, C. P.; Vezin, H.; Sougrati, M. T.; Doublet, M. L.; Foix, D.; Gonbeau, D.; Walker, W.; Prakash, A. S.; Ben Hassine, M.; Dupont, L.; Tarascon, J. M. Reversible Anionic Redox Chemistry in High-Capacity Layered-Oxide Electrodes. *Nat. Mater.* **2013**, *12*, 827−835.
(15) Foix, D.; Sathiya, M.; McCalla, E.; Tarascon, J. M.; Gonbeau, D. X-ray Photoemission Spectroscopy Study of Cationic and Anionic Redox Processes in High-Capacity Li-ion Battery Layered-Oxide Electrodes. *J. Phys. Chem. C* **2016**, *120*, 862−874.
(16) Assat, G.; Foix, D.; Delacourt, C.; Iadecola, A.; Dedryvère, R.; Tarascon, J.-M. Fundamental Interplay between Anionic/Cationic Redox Governing the Kinetics and Thermodynamics of Lithium-Rich Cathodes. *Nat. Commun.* **2017**, *8*, 2219.
(17) Yang, W.; Devereaux, T. P. Anionic and Cationic Redox and Interfaces in Batteries: Advances from Soft X-ray Absorption Spectroscopy to Resonant Inelastic Scattering. *J. Power Sources* **2018**, *389*, 188−197.
(18) Dai, K.; Wu, J.; Zhuo, Z.; Li, Q.; Sallis, S.; Mao, J.; Ai, G.; Sun, C.; Li, Z.; Gent, W. E.; Chueh, W. C.; Chuang, Y.; Zeng, R.; Shen, Z.; Pan, F.; Yan, S.; Piper, L. F.; Hussain, Z.; Liu, G.; Yang, W. High Reversibility of Lattice Oxygen Redox Quantified by Direct Bulk Probes of Both Anionic and Cationic Redox Reactions. *Joule* **2019**, *3*, 518−541.
(19) Perez, A. J.; Batuk, D.; Saubanère, M.; Rousse, G.; Foix, D.; McCalla, E.; Berg, E. J.; Dugas, R.; H. W. van den Bos, K.; Doublet, M.-L.; Gonbeau, D.; Abakumov, A. M.; Van Tendeloo, G.; Tarascon, J.-M. Strong Oxygen Participation in the Redox Governing the Structural and Electrochemical Properties of Na-Rich Layered Oxide Na_2IrO_3. *Chem. Mater.* **2016**, *28*, 8278−8288.
(20) Rong, X.; Liu, J.; Hu, E.; Liu, Y.; Wang, Y.; Wu, J.; Yu, X.; Page, K.; Hu, Y.-S.; Yang, W.; Li, H.; Yang, X.-Q.; Chen, L.; Huang, X. Structure-Induced Reversible Anionic Redox Activity in Na Layered Oxide Cathode. *Joule* **2018**, *2*, 125−140.
(21) Qiao, Y.; Guo, S.; Zhu, K.; Liu, P.; Li, X.; Jiang, K.; Sun, C.-J.; Chen, M.; Zhou, H. Reversible Anionic Redox Activity in Na_3RuO_4 Cathodes: a Prototype Na-Rich Layered Oxide. *Energy Environ. Sci.* **2018**, *11*, 299−305.
(22) Li, Q.; Qiao, Y.; Guo, S.; Jiang, K.; Li, Q.; Wu, J.; Zhou, H. Both Cationic and Anionic Co-(de)intercalation into a Metal-Oxide Material. *Joule* **2018**, *2*, 1134−1145.
(23) Li, X.; Qiao, Y.; Guo, S.; Xu, Z.; Zhu, H.; Zhang, X.; Yuan, Y.; He, P.; Ishida, M.; Zhou, H. Direct Visualization of the Reversible O^{2-}/O^{-} Redox Process in Li-Rich Cathode Materials. *Adv. Mater.* **2018**, *30*, 1705197.
(24) Zhang, X.; Qiao, Y.; Guo, S.; Jiang, K.; Xu, S.; Xu, H.; Wang, P.; He, P.; Zhou, H. Manganese-Based Na-Rich Materials Boost Anionic Redox in High-Performance Layered Cathodes for Sodium-Ion Batteries. *Adv. Mater.* **2019**, *31*, 1807770.
(25) Taylor, Z. N.; Perez, A. J.; Coca-Clemente, J. A.; Braga, F.; Drewett, N. E.; Pitcher, M. J.; Thomas, W. J.; Dyer, M. S.; Collins, C.; Zanella, M.; Johnson, T.; Day, S.; Tang, C.; Dhanak, V. R.; Claridge, J. B.; Hardwick, L. J.; Rosseinsky, M. J. Stabilization of O-O Bonds by d^0 Cations in $Li_x^{4+}Ni_{1-x}WO_6$ $(0 \leq x \leq 0.25)$ Rock Salt Oxides as the Origin of Large Voltage Hysteresis. *J. Am. Chem. Soc.* **2019**, *141*, 7333−7346.
(26) Uchimoto, Y.; Tanida, H.; Matsunaga, T.; Minato, T.; Nakanishi, K.; Ukyo, Y.; Komatsu, H.; Shimoda, K.; Ogumi, Z.; Arai, H. Oxidation Behaviour of Lattice Oxygen in Li-Rich Manganese-Based Layered Oxide Studied by Hard X-ray Photoelectron Spectroscopy. *J. Mater. Chem. A* **2016**, *4*, 5909−5916.
(27) Assat, G.; Iadecola, A.; Foix, D.; Dedryvère, R.; Tarascon, J.-M. Direct Quantification of Anionic Redox over Long Cycling of Li-Rich NMC via Hard X-ray Photoemission Spectroscopy. *ACS Energy Lett.* **2018**, *3*, 2721−2728.
(28) Dupin, J.-C.; Gonbeau, D.; Vinatier, P.; Levasseur, A. Systematic XPS Studies of Metal Oxides, Hydroxides and Peroxides. *Phys. Chem. Chem. Phys.* **2000**, *2*, 1319−1324.
(29) Yao, K. P. C.; Kwabi, D. G.; Quinlan, R. A.; Mansour, A. N.; Grimaud, A.; Lee, Y.-L.; Lu, Y.-C.; Shao-Horn, Y. Thermal Stability of Li_2O_2 and Li_2O for Li-Air Batteries: In Situ XRD and XPS Studies. *J. Electrochem. Soc.* **2013**, *160*, A824−A831.
(30) Rana, J.; Papp, J. K.; Lebens-Higgins, Z.; Zuba, M.; Kaufman, L. A.; Goel, A.; Schmuch, R.; Winter, M.; Whittingham, M. S.; Yang, W.; McCloskey, B. D.; Piper, L. F. J. Quantifying the Capacity Contributions during Activation of Li_2MnO_3. *ACS Energy Letters* **2020**, *5*, 634−641.
(31) Lebens-Higgins, Z. W.; Vinckeviciute, J.; Wu, J.; Faenza, N. V.; Li, Y.; Sallis, S.; Pereira, N.; Meng, Y. S.; Amatucci, G. G.; Der Ven, A. V.; Yang, W.; Piper, L. F. J. Distinction between Intrinsic and X-ray-Induced Oxidized Oxygen States in Li-Rich 3d Layered Oxides and $LiAlO_2$. *J. Phys. Chem. C* **2019**, *123*, 13201−13207.

(32) Chung, H.; Grenier, A.; Huang, R.; Wang, X.; Lebens-Higgins, Z.; Doux, J.-m.; Sallis, S.; Song, C.; Ercius, P.; Chapman, K.; Piper, L. F. J.; Cho, H.-m.; Zhang, M.; Meng, Y. S. Comprehensive Study of a Versatile Polyol Synthesis Approach for Cathode Materials for Li-Ion Batteries. *Nano Res.* **2019**, *12*, 2238−2249.
(33) Shinotsuka, H.; Tanuma, S.; Powell, C. J.; Penn, D. R. Calculations of Electron Inelastic Mean Free Paths. X. Data for 41 Elemental Solids over the 50 eV to 200 keV Range with the Relativistic Full Penn Algorithm. *Surf. Interface Anal.* **2015**, *47*, 871−888.
(34) Powell, C. J.; Jablonski, A. *NIST Electron Inelastic-Mean-Free-Path Database*, version 1.2, SRD 71; National Institute of Standards and Technology: Gaithersburg, MD, 2010.
(35) Jablonski, A.; Powell, C. J. Information Depth and the Mean Escape Depth in Auger Electron Spectroscopy and X-ray Photoelectron Spectroscopy. *J. Vac. Sci. Technol., A* **2003**, *21*, 274−283.
(36) Hwang, S.; Chang, W.; Kim, S. M.; Su, D.; Kim, D. H.; Lee, J. Y.; Chung, K. Y.; Stach, E. A. Investigation of Changes in the Surface Structure of $Li_xNi_{0.8}Co_{0.15}Al_{0.05}O_2$ Cathode Materials Induced by the Initial Charge. *Chem. Mater.* **2014**, *26*, 1084−1092.
(37) Carroll, K. J.; Qian, D.; Fell, C.; Calvin, S.; Veith, G. M.; Chi, M.; Baggetto, L.; Meng, Y. S. Probing the Electrode/Electrolyte Interface in the Lithium Excess Layered Oxide $Li_{1.2}Ni_{0.2}Mn_{0.6}O_2$. *Phys. Chem. Chem. Phys.* **2013**, *15*, 11128−11138.
(38) Lin, F.; Markus, I. M.; Nordlund, D.; Weng, T.-C.; Asta, M. D.; Xin, H. L.; Doeff, M. M. Surface Reconstruction and Chemical Evolution of Stoichiometric Layered Cathode Materials for Lithium-Ion Batteries. *Nat. Commun.* **2014**, *5*, 3529.
(39) Oishi, M.; Yamanaka, K.; Watanabe, I.; Shimoda, K.; Matsunaga, T.; Arai, H.; Ukyo, Y.; Uchimoto, Y.; Ogumi, Z.; Ohta, T. Direct Observation of Reversible Oxygen Anion Redox Reaction in Li-Rich Manganese Oxide, Li_2MnO_3, Studied by Soft X-ray Absorption spectroscopy. *J. Mater. Chem. A* **2016**, *4*, 9293−9302.
(40) Zheng, J.; Xu, P.; Gu, M.; Xiao, J.; Browning, N. D.; Yan, P.; Wang, C.; Zhang, J.-G. Structural and Chemical Evolution of Li- and Mn-Rich Layered Cathode Material. *Chem. Mater.* **2015**, *27*, 1381−1390.
(41) Biesinger, M. C.; Payne, B. P.; Grosvenor, A. P.; Lau, L. W. M.; Gerson, A. R.; Smart, R. S. C. Resolving Surface Chemical States in XPS Analysis of First Row Transition Metals, Oxides and Hydroxides: Cr, Mn, Fe, Co and Ni. *Appl. Surf. Sci.* **2011**, *257*, 2717−2730.
(42) Nelson, A. J.; Reynolds, J. G.; Roos, J. W. Core-Level Satellites and Outer Core-Level Multiplet Splitting in Mn Model Compounds. *J. Vac. Sci. Technol., A* **2000**, *18*, 1072−1076.
(43) Ilton, E. S.; Post, J. E.; Heaney, P. J.; Ling, F. T.; Kerisit, S. N. XPS Determination of Mn Oxidation States in Mn (hydr)oxides. *Appl. Surf. Sci.* **2016**, *366*, 475−485.
(44) Lebens-Higgins, Z. W.; Sallis, S.; Faenza, N. V.; Badway, F.; Pereira, N.; Halat, D. M.; Wahila, M.; Schlueter, C.; Lee, T.-L.; Yang, W.; Grey, C. P.; Amatucci, G. G.; Piper, L. F. J. Evolution of the Electrode-Electrolyte Interface of $LiNi_{0.8}Co_{0.15}Al_{0.05}O_2$ Electrodes due to Electrochemical and Thermal Stress. *Chem. Mater.* **2018**, *30*, 958−969.
(45) Grenier, A.; Liu, H.; Wiaderek, K. M.; Lebens-Higgins, Z. W.; Borkiewicz, O. J.; Piper, L. F. J.; Chupas, P. J.; Chapman, K. W. Reaction Heterogeneity in $LiNi_{0.8}Co_{0.15}Al_{0.05}O_2$ Induced by Surface Layer. *Chem. Mater.* **2017**, *29*, 7345−7352.
(46) Zhang, K. H. L.; Du, Y.; Sushko, P. V.; Bowden, M. E.; Shutthanandan, V.; Sallis, S.; Piper, L. F. J.; Chambers, S. A. Hole-Induced Insulator-to-Metal Transition in $La_{1-x}Sr_xCrO_3$ Epitaxial Films. *Phys. Rev. B: Condens. Matter Mater. Phys.* **2015**, *91*, 155129.
(47) Fujimori, A.; Ino, A.; Matsuno, J.; Yoshida, T.; Tanaka, K.; Mizokawa, T. Core-Level Photoemission Measurements of the Chemical Potential Shift as a Probe of Correlated Electron Systems. *J. Electron Spectrosc. Relat. Phenom.* **2002**, *124*, 127−138.
(48) Massel, F.; Hikima, K.; Rensmo, H.; Suzuki, K.; Hirayama, M.; Xu, C.; Younesi, R.; Liu, Y.-S.; Guo, J.; Kanno, R.; Hahlin, M.; Duda, L.-C. Excess Lithium in Transition Metal Layers of Epitaxially Grown Thin Film Cathodes of Li 2 MnO 3 Leads to Rapid Loss of Covalency during First Battery Cycle. *J. Phys. Chem. C* **2019**, *123*, 28519−28526.
(49) Yu, D. Y. W.; Yanagida, K.; Kato, Y.; Nakamura, H. Electrochemical Activities in Li_2MnO_3. *J. Electrochem. Soc.* **2009**, *156*, A417.
(50) Verdier, S.; El Ouatani, L.; Dedryvére, R.; Bonhomme, F.; Biensan, P.; Gonbeau, D. XPS Study on Al_2O_3- and $AlPO_4$-Coated $LiCoO_2$ Cathode Material for High-Capacity Li Ion Batteries. *J. Electrochem. Soc.* **2007**, *154*, A1088−A1099.
(51) Lu, Y. C.; Mansour, A. N.; Yabuuchi, N.; Shao-Horn, Y. Probing the Origin of Enhanced Stability of $AlPO_4$ Nanoparticle Coated $LiCoO_2$ during Cycling to High Voltages: Combined XRD and XPS Studies. *Chem. Mater.* **2009**, *21*, 4408−4424.
(52) Zhang, J. N.; Li, Q.; Ouyang, C.; Yu, X.; Ge, M.; Huang, X.; Hu, E.; Ma, C.; Li, S.; Xiao, R.; Yang, W.; Chu, Y.; Liu, Y.; Yu, H.; Yang, X. Q.; Huang, X.; Chen, L.; Li, H. Trace Doping of Multiple Elements Enables Stable Battery Cycling of $LiCoO_2$ at 4.6 V. *Nat. Energy* **2019**, *4*, 594.
(53) Dogan, F.; Croy, J. R.; Balasubramanian, M.; Slater, M. D.; Iddir, H.; Johnson, C. S.; Vaughey, J. T.; Key, B. Solid state NMR studies of Li_2MnO_3 and li-rich cathode materials: Proton insertion, local structure, and voltage fade. *J. Electrochem. Soc.* **2015**, *162*, A235−A243.
(54) Renfrew, S. E.; McCloskey, B. D. Residual Lithium Carbonate Predominantly Accounts for First Cycle CO_2 and CO Outgassing of Li-Stoichiometric and Li-Rich Layered Transition-Metal Oxides. *J. Am. Chem. Soc.* **2017**, *139*, 17853−17860.
(55) Lebens-Higgins, Z. W.; Faenza, N. V.; Radin, M. D.; Liu, H.; Sallis, S.; Rana, J.; Vinckeviciute, J.; Reeves, P. J.; Zuba, M. J.; Badway, F.; Pereira, N.; Chapman, K. W.; Lee, T.-L.; Wu, T.; Grey, C. P.; Melot, B. C.; Van Der Ven, A.; Amatucci, G. G.; Yang, W.; Piper, L. F. J. Revisiting the Charge Compensation Mechanisms in $Li-Ni_{0.8}Co_{0.2-y}Al_yO_2$ Systems. *Mater. Horiz.* **2019**, *6*, 2112−2123.
(56) Qiao, R.; Wang, Y.; Olalde-Velasco, P.; Li, H.; Hu, Y. S.; Yang, W. Direct Evidence of Gradient Mn(II) Evolution at Charged States in $LiNi_{0.5}Mn_{1.5}O_4$ Electrodes with Capacity Fading. *J. Power Sources* **2015**, *273*, 1120−1126.
(57) Li, Q.; Qiao, R.; Wray, L. A.; Chen, J.; Zhuo, Z.; Chen, Y.; Yan, S.; Pan, F.; Hussain, Z.; Yang, W. Quantitative Probe of the Transition Metal Redox in Battery Electrodes through Soft X-ray Absorption Spectroscopy. *J. Phys. D: Appl. Phys.* **2016**, *49*, 413003.
(58) Renfrew, S. E.; McCloskey, B. D. Quantification of Surface Oxygen Depletion and Solid Carbonate Evolution on the First Cycle of $LiNi_{0.6}Mn_{0.2}Co_{0.2}O_2$ Electrodes. *ACS Appl. Energy Mater.* **2019**, *2*, 3762−3772.